JACS
JOURNAL OF THE AMERICAN CHEMICAL SOCIETY
Article
pubs.acs.org/JACS

Determining Relative f and d Orbital Contributions to M−Cl Covalency in MCl_6^{2-} (M = Ti, Zr, Hf, U) and $UOCl_5^-$ Using Cl K-Edge X-ray Absorption Spectroscopy and Time-Dependent Density Functional Theory

Stefan G. Minasian,[†,‡] Jason M. Keith,[†] Enrique R. Batista,*[,†] Kevin S. Boland,[†] David L. Clark,*[,†] Steven D. Conradson,*[,†] Stosh A. Kozimor,*[,†] Richard L. Martin,*[,†] Daniel E. Schwarz,[†] David K. Shuh,[‡] Gregory L. Wagner,[†] Marianne P. Wilkerson,[†] Laura E. Wolfsberg,[†] and Ping Yang[§]

[†]Los Alamos National Laboratory, Los Alamos, New Mexico 87545, United States

[‡]Chemical Sciences Division, Lawrence Berkeley National Laboratory, Berkeley, California 94720, United States

[§]W.R. Wiley Environmental Molecular Sciences Laboratory, Pacific Northwest National Laboratory, Richland, Washington 99352, United States

Supporting Information

ABSTRACT: Chlorine K-edge X-ray absorption spectroscopy (XAS) and ground-state and time-dependent hybrid density functional theory (DFT) were used to probe the electronic structures of O_h-MCl_6^{2-} (M = Ti, Zr, Hf, U) and C_{4v}-$UOCl_5^-$, and to determine the relative contributions of valence 3d, 4d, 5d, 6d, and 5f orbitals in M−Cl bonding. Spectral interpretations were guided by time-dependent DFT calculated transition energies and oscillator strengths, which agree well with the experimental XAS spectra. The data provide new spectroscopic evidence for the involvement of both 5f and 6d orbitals in actinide−ligand bonding in UCl_6^{2-}. For the MCl_6^{2-}, where transitions into d orbitals of t_{2g} symmetry are spectroscopically resolved for all four complexes, the experimentally determined Cl 3p character per M−Cl bond increases from 8.3(4)% ($TiCl_6^{2-}$) to 10.3(5)% ($ZrCl_6^{2-}$), 12(1)% ($HfCl_6^{2-}$), and 18(1)% (UCl_6^{2-}). Chlorine K-edge XAS spectra of $UOCl_5^-$ provide additional insights into the transition assignments by lowering the symmetry to C_{4v}, where five pre-edge transitions into both 5f and 6d orbitals are observed. For UCl_6^{2-}, the XAS data suggest that orbital mixing associated with the U 5f orbitals is considerably lower than that of the U 6d orbitals. For both UCl_6^{2-} and $UOCl_5^-$, the ground-state DFT calculations predict a larger 5f contribution to bonding than is determined experimentally. These findings are discussed in the context of conventional theories of covalent bonding for d- and f-block metal complexes.

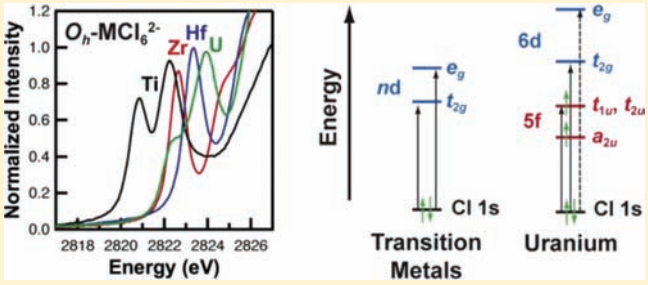

INTRODUCTION

The covalent sharing of electrons between elements is fundamental to descriptions of electronic structure and bonding.[1] For d-block metal complexes, many studies indicate that differences in covalent orbital mixing between metal orbitals and appropriate ligand orbitals are closely correlated to differences in their chemical reactivities and physical properties.[2−5] Whether the f-block elements engage in covalent bonding is still uncertain, and unraveling the nature of bonding in systems containing actinides and lanthanides remains a computational and experimental challenge.[6,7] This is especially true for the 5f elements, where many studies using optical spectroscopy have supported the viewpoint that 5f orbitals are core-like, only weakly perturbed by ligand fields, and not generally involved in covalent bonding.[8] Yet, while such studies indicate that ionic models can provide reasonable bonding descriptions of 5f elements in certain chemical environments, there are also numerous reports where actinides show evidence of covalent bonding interactions.[9−20] For example, a large body of work has demonstrated both 5f and 6d orbitals are involved in covalent U≡O triple bonds in the uranyl ion, UO_2^{2+},[21−24] and in the U−C bonds to the $C_8H_8^{2-}$ rings in uranocene, $(C_8H_8)_2U$.[11,25−32] Differences in covalency have also been invoked to rationalize the observation that soft donor S- and N-based ligands are highly selective in separating trivalent actinides from lanthanides in nuclear fuel reprocessing.[33−41] Theoretical studies on actinide molecular systems suggest that the 6d orbitals play a significant—and perhaps dominant—role in actinide bonding relative to the 5f orbitals.[11,16,18,42,43] Nevertheless, current theories of actinide bonding are limited by a lack of experimental approaches to probe 5f and 6d orbital covalency with a broad class of ligands.

Received: November 8, 2011
Published: March 9, 2012

   dx.doi.org/10.1021/ja2105015 | J. Am. Chem. Soc. 2012, 134, 5586−5597

Of the experimental approaches to determine covalency, ligand K-edge X-ray absorption spectroscopy (XAS) has emerged as an effective method for measuring orbital mixing in metal−ligand bonds.[44−50] This technique has been used extensively in the study of d-block systems,[44−46,49,51−56] and was recently extended to the actinides.[23,57] In ligand K-edge XAS, bound state transitions can occur on the low-energy side of the absorption edge involving the excitation of 1s electrons (localized on the ligand) into singly occupied or unoccupied acceptor orbitals of the metal complex. The presence of covalent mixing is observed as a pre-edge peak in the ligand K-edge XAS, and can only have transition intensity if the empty metal orbital (in this case f or d) contains a significant component of ligand p character.[44−50] Hence, this technique affords an opportunity to quantify the degree of covalency and assess the relative roles of valence f and d orbitals in actinide metal−ligand bonds.

To evaluate metal and ligand orbital mixing as a function of the 3d, 4d, 5d, 5f, and 6d metal orbitals, we recently reported a Cl K-edge XAS and time-dependent density functional theory (TD-DFT) study on a series of structurally related $(C_5Me_5)_2MCl_2$ (M = Ti, Zr, Hf, Th, U) complexes.[57] That study provided direct evidence of 5f orbital mixing in the U−Cl bonds, but the 6d orbital contribution could not be rigorously evaluated. The goal of the present study is to provide insight into the relative roles of 5f vs 6d orbitals in metal−ligand bonding by evaluating a series of octahedral MCl_6^{2-} complexes (M = Ti, Zr, Hf, U) and pseudo-octahedral $UOCl_5^-$ using Cl K-edge XAS and TD-DFT. These highly symmetric complexes were carefully chosen because their electronic structure is the foundation upon which much of the current understanding of metal−ligand bonding is based.[2,4,5] Because the MCl_6^{2-} complexes have the same geometry, identification of transitions associated with the Ti, Zr, and Hf d orbitals should provide a sound basis for identifying transitions associated with the 5f and 6d orbitals in UCl_6^{2-}. In addition, optical spectroscopies suggest that the 5f and 6d orbitals are well-separated energetically in $UOCl_5^-$ and UCl_6^{2-}, which should facilitate excited-state spectral interpretations despite the significant differences in ground-state electronic structure.[8,22] An additional mechanism for verifying 5f and 6d orbital participation in bonding is also available through comparison of UCl_6^{2-} to $UOCl_5^-$ because the stepwise symmetry reduction from O_h to C_{4v} lifts the degeneracy in a significant and predictable fashion.

RESULTS AND DISCUSSION

Sample Preparation. All Cl K-edge XAS experiments were conducted on metal chloride anions that contained non-coordinating countercations (i.e., Ph_4P^+, Et_4N^+, and Bu_4N^+) to ensure that the anions are isolated and to prevent bridging M−Cl−M interactions. These complexes can be prepared in large quantities and isolated as highly pure crystalline solids.[58] Each sample was encapsulated in a polystyrene matrix, such that the total amount of chlorine was approximately 4×10^{-5} mol of Cl per mg of total sample. Previous work suggests that this ratio provides balance in maximizing signal-to-noise while minimizing X-ray self-absorption.[53,57] Encapsulation in a polystyrene matrix also provides a safe method for containment of radioactive samples without requiring implementation of windows, special chambers, or other traditional radiological barriers that can attenuate the incident radiation and sample fluorescence. For UCl_6^{2-} and $UOCl_5^-$, the spectra obtained on samples encapsulated in polystyrene were identical to those from samples prepared as thin films of powder dispersed on Kapton tape, confirming that the polystyrene matrix has no noticeable effect on room-temperature Cl K-edge XAS data.[53]

Cl K-Edge XAS. The background-subtracted and normalized chlorine K-edge XAS of MCl_6^{2-} (M = Ti, Zr, Hf, U) and $UOCl_5^-$ are shown in Figure 1. These spectra are similar to those observed previously for $(C_5Me_5)_2MCl_2$ (M = Ti, Zr, Hf, Th, U) in that distinct pre-edge features indicative of covalent M−Cl interactions are apparent between 2820 and 2826 eV.[49,53,57] It is instructive to first consider the origin of the pre-edge features in the d-block MCl_6^{2-} spectra before discussing the data for UCl_6^{2-} and $UOCl_5^-$. For $TiCl_6^{2-}$, two well-resolved pre-edge features are observed at 2820.80 and 2822.25 eV. Similar spectra are observed for $ZrCl_6^{2-}$ and $HfCl_6^{2-}$ (Figure 1 and Table 1), with the exception that the pre-edge peaks are shifted to higher energy and the second features are best described as pre-edge shoulders on the rising edge. A similar observation was reported for the $(C_5R_5)_2MCl_2$ systems (R = H, Me; M = Ti, Zr, Hf), and in all three cases the increase in pre-edge peak energies is attributed to the increasing energy of the 3d, 4d, and 5d orbital final states.[53,57]

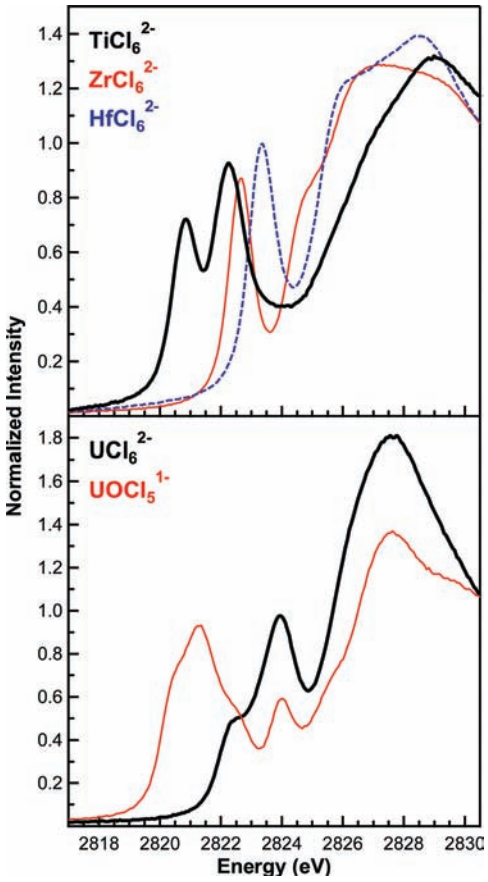

Figure 1. Cl K-edge fluorescence yield spectra obtained for polystyrene encapsulated samples of $(Ph_4P)_2MCl_6$ (M = Ti, top, thick black trace; Zr, top, thin red trace; Hf, top, dashed blue trace; U, bottom, thick black trace) and $(Et_4N)UOCl_5$ (bottom, thin red trace).

The spectral features for d-block MCl_6^{2-} (M = Ti, Zr, Hf) were modeled as previously described using pseudo-Voigt line shapes, which are composed of a 1:1 ratio of Lorentzian to Gaussian functions of equal height and width (Figure 2 and Table 1).[50,53,57] The line shape for the rising edge was calculated by subtracting the pre-edge features from the spectral

dx.doi.org/10.1021/ja2105015 | J. Am. Chem. Soc. 2012, 134, 5586−5597

Table 1. Comparison of Experimental and Calculated Cl K-Edge Pre-edge Peak Energies (eV),[a] Intensities (Int), Oscillator Strengths (f),[b] and Contribution of Cl 3p to Bonding (%)[c] for Polystyrene-Encapsulated Samples of $(Ph_4P)_2MCl_6$ (M = Ti, Zr, Hf, U) and $(Et_4N)UOCl_5$

		energy, eV				% Cl 3p per bond	
compd	assignment	exptl	calcd[a]	Int	f, calcd[b]	exptl	calcd[c]
D_{2d}-$CuCl_4^{2-}$	$1s \rightarrow b_{1g}$	2820.21[d]	–	0.53[d]	–	7.5[d]	–
O_h-$TiCl_6^{2-}$	$1s \rightarrow t_{2g}$	2820.80	2820.88	0.58(3)	0.0063	8.3(4)	12.3
	$1s \rightarrow e_g$	2822.25	2822.18	0.99(5)	0.0073	14(1)	11.1
O_h-$ZrCl_6^{2-}$	$1s \rightarrow t_{2g}$	2822.64	2822.63	0.73(3)	0.0060	10.3(5)	11.1
	$1s \rightarrow e_g$	2824.66	2824.73	*e*	0.0066	*e*	8.7
O_h-$HfCl_6^{2-}$	$1s \rightarrow t_{2g}$	2823.34	2823.37	0.88(4)	0.0060	12(1)	10.2
	$1s \rightarrow e_g$	2825.70	2825.67	*e*	0.0066	*e*	8.2
O_h-UCl_6^{2-}	$1s \rightarrow t_{2u} + t_{1u}$	2822.41	2821.27, 2822.17	0.40(2)	0.0025, 0.0018	5.7(3)	22.5
	$1s \rightarrow t_{2g}$	2823.88	2823.70, 2824.13	1.24(6)	0.0017, 0.0022	18(1)	6.5
	$1s \rightarrow e_g$	*e*	2826.56	*e*	0.0014	*e*	5.7
C_{4v}-$UOCl_5^-$	$1s \rightarrow b_1$ (t_{2u})	2820.35	2820.29	0.26(1)	0.0012	3.7(2)	2.0
	$1s \rightarrow e + e$ ($t_{2u} + t_{1u}$)	2821.29	2820.40, 2820.93, 2821.47	1.26(6)	0.0034, 0.0015, 0.0010	18(1)	29.0
	$1s \rightarrow a_1$ (t_{1u})	2822.57	2822.09	0.29(1)	0.0018	4.2(2)	16.3
	$1s \rightarrow b_2$ (t_{2g})	2823.99	2823.99	0.37(2)	0.0020	5.3(3)	2.7
	$1s \rightarrow e$ (t_{2g})	2825.31	2825.76, 2826.36	0.14(1)	0.0013, 0.0010	2.0(1)	4.3
	$1s \rightarrow b_1$ (e_g)	*e*	2827.23	*e*	0.0012	*e*	5.5
	$1s \rightarrow a_1$ (e_g)	*e*	2828.62	*e*	0.0008	*e*	4.7

[a]Calculated values are taken from the TD-DFT simulated spectra (see Experimental Section). More transitions are often observed in the calculated spectra than are independently resolved by experiment. [b]Oscillator strengths are taken from the TD-DFT calculations and are uncorrected. [c]The % Cl 3p per bond values were determined by multiplying the total Cl 3p character by the sum of the squares of the normalization constants for the corresponding ligand-orbital wave functions (see Experimental Section). [d]Ref 50. [e]An accurate intensity or energy for this transition could not be determined experimentally.

data. For $TiCl_6^{2-}$, the first and second derivatives of the data (see the Supporting Information) and the curve-fitting analysis suggest that another high-energy feature is present between the peak at 2822.25 eV and the rising edge, and an appropriate model of the data required addition of a third pre-edge function at 2823.60 eV. In contrast, spectra of $ZrCl_6^{2-}$ and $HfCl_6^{2-}$ were modeled satisfactorily with only two pre-edge functions. The low-energy features at 2822.64 and 2823.34 eV for $ZrCl_6^{2-}$ and $HfCl_6^{2-}$, respectively, are well resolved, and the intensities can be determined with high confidence. The close proximity of the second, higher-energy features to the rising edge results in greater uncertainty in the intensity of their corresponding curve fit functions. This produces significant variability in pre-edge shoulder intensities, because a number of models provide good approximations of the experimental data. Consequently, only the intensities for the first peak in the Zr and Hf systems are discussed (Table 1).

The Cl K-edge XAS of UCl_6^{2-} is similar to the spectra of $ZrCl_6^{2-}$ and $HfCl_6^{2-}$ in that it also has two pre-edge features (Figure 2), and differs in that the first pre-edge feature is less intense than the second. Second derivative spectra also indicate the presence of an additional high-energy shoulder on the rising edge. The first UCl_6^{2-} pre-edge feature at 2822.41 eV is lower in energy than those derived from transitions into d orbitals in the spectra of $ZrCl_6^{2-}$ and $HfCl_6^{2-}$. A similar observation was made previously in the Cl K-edge XAS of $(C_5Me_5)_2UCl_2$, where the low-energy feature was attributed to transitions to U 5f orbitals.[57] The spectrum for $UOCl_5^-$ is distinct from all the MCl_6^{2-} spectra because it contains multiple pre-edge features between 2820 to 2824 eV and a shoulder on the rising edge near 2825.31 eV. In addition, for $UOCl_5^-$ the most intense pre-edge feature is low in energy (2821.29 eV), whereas for UCl_6^{2-} the most intense pre-edge feature is at high energy (2823.88 eV). Using the second derivatives as a guide to generate a model for the spectrum of $UOCl_5^-$, a high-quality curve fit for the pre-edge region was obtained that included five pre-edge functions (Figure 2 and Table 1). This model is unusual in that Cl K-edge XAS of monomeric complexes with terminal chloride ligands typically exhibit only one or two pre-edge features.[44−46,49,53,57,59] Given that it is impossible to rationalize a spectrum for a C_{4v}-symmetric complex with five easily resolved pre-edge features by invoking only 6d orbital participation in bonding, it seems likely that transitions involving both 5f and 6d orbitals are present in the Cl K-edge XAS for $UOCl_5^-$ as well as for UCl_6^{2-}. For additional guidance into the origins of the pre-edge transitions shown in Figure 2, electronic structure calculations were conducted on the MCl_6^{2-} and $UOCl_5^-$ complexes.

Ground-State Electronic Structure Calculations. The origins of the pre-edge transitions in the Cl K-edge XAS shown in Figures 1 and 2 can be evaluated by considering the molecular orbital interactions for each complex.[2,4,5] For a transition metal in an octahedral ligand field, the six Cl 3p σ-orbitals span $a_{1g} + e_g + t_{1u}$ symmetries and can form six M−Cl σ-bonds using the M valence s, p, and d orbitals of the same symmetry. The remaining 12 Cl 3p orbitals of π-symmetry with respect to the M−Cl bonds transform as $t_{1g} + t_{2g} + t_{1u} + t_{2u}$ symmetries.[2,4,5,60] In the general model for transition metals,

dx.doi.org/10.1021/ja2105015 | J. Am. Chem. Soc. 2012, 134, 5586−5597

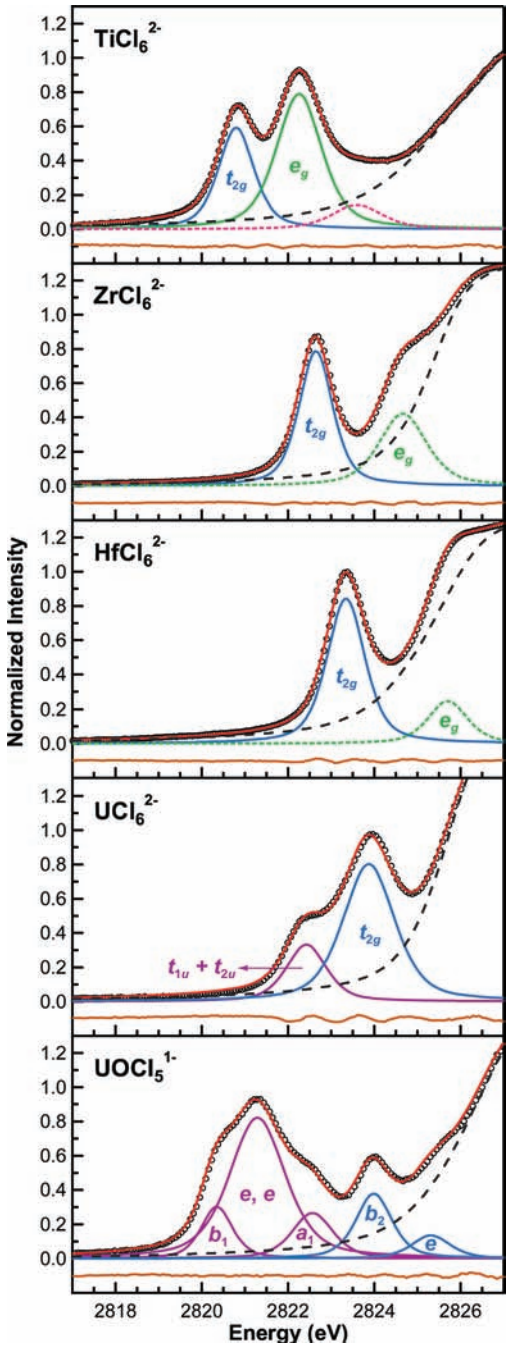

Figure 2. Cl K-edge fluorescence yield experimental data (black circles), and pseudo-Voigt functions (blue, green, purple, and pink traces) used to generate the curve fits (red traces) for polystyrene-encapsulated samples of $(Ph_4P)_2MCl_6$ (M = Ti, Zr, Hf, U) and $(Et_4N)UOCl_5$. Post-edge residual data (dashed gray traces) are equal to the experimental data minus the pseudo-Voigt functions. Total residual data (orange traces, offset) are equal to the experimental data minus the curve fit.

the t_{1g}, t_{1u}, and t_{2u} orbitals represent the nonbonding Cl lone pairs, while the t_{2g} set can form M−Cl π-bonds using metal d orbitals. This gives the well-known e_g and t_{2g} d orbitals that are σ- and π-antibonding with respect to the M−Cl interactions. In the Cl K-edge XAS, only transitions associated with spin- and electric-dipole-allowed final states will be observed. Because each of the d^0 transition metal MCl_6^{2-} has a $^1A_{1g}$ ground state and the electric dipole operator in O_h symmetry is t_{1u}, transitions must be between $^1A_{1g} \rightarrow {}^1T_{1u}$ states. The first and second pre-edge features in the Cl K-edge XAS of MCl_6^{2-} (M = Ti, Zr, Hf) are therefore reasonably assigned to excitations from the linear combination of Cl 1s-based orbitals having t_{1u} symmetry to empty metal d orbitals of t_{2g} and e_g symmetries.

This qualitative interpretation is consistent with the quantitative molecular orbital picture obtained using ground-state DFT calculations. Because the occupied molecular orbitals for MCl_6^{2-} complexes are well known,[5] this discussion focuses primarily on the α spin−orbital energies and atomic orbital compositions of the unoccupied metal-based orbitals that are relevant to the Cl K-edge XAS (Figure 3 and Table 2). As

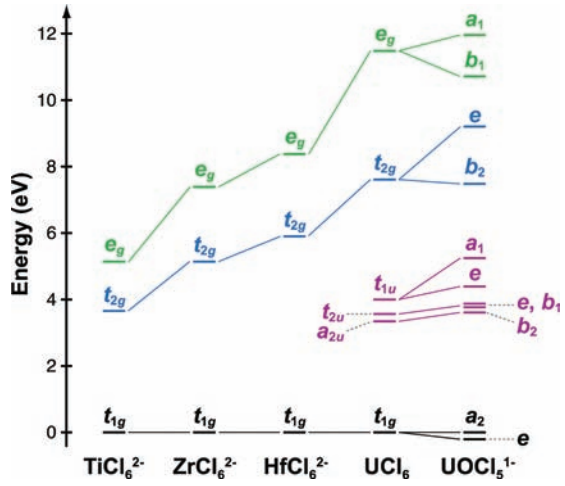

Figure 3. Correlation of the calculated molecular orbital diagrams for MCl_6^{2-} (M = Ti, Zr, Hf), UCl_6, and $UOCl_5^-$ showing the HOMO and unoccupied orbitals that have primarily *n*d character (blue and green), and orbitals with primarily 5f character (purple). Molecular orbitals energies are based on the data in Table 2, but have been shifted by a constant so that each HOMO has energy of 0 eV.

expected, in each calculation the HOMO consists of non-bonding Cl-based lone pairs of t_{1g} symmetry. At higher energy are the unoccupied primarily metal d LUMOs of t_{2g} symmetry, which are M−Cl π-antibonding. The calculated HOMO−LUMO gaps increase from 3.65 to 5.14 and to 5.90 eV for MCl_6^{2-} (M = Ti, Zr, and Hf, respectively), as expected from previously reported charge-transfer spectra (3.72, 4.17, and 4.53 eV).[61,62] Consistent with the experimental data, the calculations also find that the molecular orbitals of t_{2g} symmetry move to higher energy with the increasing energy of the d orbitals along the series Ti (3d), Zr (4d), and Hf (5d) (Figure 3). These MOs are composed primarily of M d orbital character, but also contain a percentage of Cl 3p orbital character due to covalent mixing: 16.4%, 14.8%, and 13.6% for $TiCl_6^{2-}$, $ZrCl_6^{2-}$, and $HfCl_6^{2-}$, respectively (Table 2).

Similarly, the calculations indicate that the e_g orbitals (M−Cl σ-antibonding) move to higher energy from $TiCl_6^{2-}$ to $HfCl_6^{2-}$, in agreement with the experimental Cl K-edge XAS data (Figure 2). The ground-state energy difference between the t_{2g} and e_g orbitals is calculated to be smallest for $TiCl_6^{2-}$ (1.48 eV), intermediate for $ZrCl_6^{2-}$ (2.25 eV), and largest for $HfCl_6^{2-}$ (2.48 eV). The experimental spectra, which provide a measure of the excited-state splittings, show an increase from $TiCl_6^{2-}$ (1.45 eV) to $ZrCl_6^{2-}$ (2.02 eV) to $HfCl_6^{2-}$ (2.36 eV). Both the DFT and XAS data for $TiCl_6^{2-}$ are in reasonable agreement with the d—d transition energies known from optical spectra of

dx.doi.org/10.1021/ja2105015 | J. Am. Chem. Soc. 2012, 134, 5586−5597

Table 2. Calculated Atomic Compositions of Selected Valence Molecular Orbitals (MOs) for MCl_6^{2-} (M = Ti, Zr, Hf, U) and $UOCl_5^-$ [a]

			MO (DFT, %)				% Cl 3p per bond	
compd	MO	energy, eV	O 2p	Cl 3p	M f	M d	calcd[b]	exptl
$TiCl_6^{2-}$	e_g	5.47	–	33.4	–	65.7	11.1	14(1)
	t_{2g}	3.99	–	16.4	–	83.2	12.3	8.3(4)
	t_{1g}	0.34	–	100	–	0	–	–
$ZrCl_6^{2-}$	e_g	7.29	–	26.2	–	74.1	8.7	–
	t_{2g}	5.04	–	14.8	–	84.2	11.1	10.3(5)
	t_{1g}	−0.10	–	100	–	0	–	–
$HfCl_6^{2-}$	e_g	8.35	–	24.6	–	76.8	8.2	–
	t_{2g}	5.87	–	13.6	–	85.1	10.2	12(1)
	t_{1g}	−0.03	–	100	–	0	–	–
UCl_6	e_g	2.37	–	29[c]	0	84.9[c]	9.7	–
	t_{2g}	−1.50	–	14.4	0	82.8	10.8	–
	t_{1u}	−5.11	–	28	71.6	0	36.6	–
	t_{2u}	−5.55	–	12.4	87.5	0	9.3	–
	a_{2u}	−5.77	–	0	99.9	0	0	–
	t_{1g}	−9.11	–	100	–	0	–	–
UCl_6^{2-}	e_g	9.84	–	17.1	0	93.3	5.7	–
	t_{2g}	6.96	–	8.8	0	89.6	6.5	18(1)
	t_{1u}	4.80	–	8.6	91.2	0	22.5	5.7(3)
	t_{2u}	4.58	–	5.5	94.8	0		
	t_{1u}	4.41	–	11.6	88	0		
	t_{2u}	1.24	–	13.2	86.7	0		
	a_{2u}	0.92	–	0	100	0	0.0	–
	t_{1g}	−0.30	–	100	–			
$UOCl_5^-$	a_1	7.62	−2.2[c]	4.7	0.8	64.0	4.7	–
	b_1	6.38	0	22.0	0	89.0	5.5	–
	e	4.86	13.0	4.3	6.0	73.7	4.3	2.0(1)
	b_2	3.14	0	10.8	0.1	87.0	2.7	5.3(3)
	a_1	0.91	16.3	18.4	56.6	6.4	16.3	4.2(2)
	e	0.05	6.3	13.0	74.2	6.2	29.0	18(1)
	e	−0.46	0.9	12.1	86.1	0.5		
	b_1	−0.61	0	8.0	92.0	0	2.0	3.7(2)
	b_2	−0.73	0	0	99.8	0.1	0	–
	a_2	−4.34	0	100	0	0	–	–

[a] α spin−orbital energies are reported. [b] The % Cl 3p per bond values were determined by dividing the total Cl 3p character by the number of bonding Cl atoms and multiplying by the molecular orbital degeneracy. [c] The use of a nonorthogonal basis set can cause Mulliken analysis to have nonphysical results such as occupations >1 or <0.[101]

the $TiCl_6^{3-}$ anion.[63,64] This excellent agreement between experiment and theory provides confidence in assigning the d-block MCl_6^{2-} pre-edge transitions in the Cl K-edge XAS to excitations that involve molecular antibonding orbitals of t_{2g} and e_g symmetries, which contain Cl 3p character due to orbital mixing.

To facilitate a comparison between $5f^2$ UCl_6^{2-} and the d^0 MCl_6^{2-} (M = Ti, Zr, Hf) complexes, the neutral UCl_6 molecule was examined by DFT because it has a closed-shell $(5f)^0(6d)^0$ ground-state electronic configuration. A molecular orbital picture for actinide hexahalides in the nonrelativistic O_h point group has been described in detail previously.[65] In an octahedral ligand field, the U 5f orbitals transform with a_{2u} + t_{2u} + t_{1u} symmetry. The U 5f orbital of a_{2u} symmetry is strictly nonbonding, the t_{2u} orbitals can form U−Cl π-bonds, and the t_{1u} orbitals can form U−Cl interactions that are both σ- and π-bonding (Figure 5). For hexavalent UCl_6, DFT shows that the HOMO consists of a nonbonding Cl-based lone pair of t_{1g} symmetry (Table 2 and Figure 3). The frontier orbitals are slightly different for tetravalent $5f^2$ UCl_6^{2-}, which is calculated to have one of its two unpaired 5f electrons in the nonbonding a_{2u} orbital (99% U 5f) and another in an antibonding t_{2u} orbital (Table 2 and Figure 4).[66] A slight energy difference for the orbitals of t_{1u} symmetry is also observed. Even with the difference in charge and electronic configuration, the DFT calculations indicate that the molecular orbital interactions of dianionic UCl_6^{2-} are quite similar to those of neutral UCl_6, which are in turn related to those of their d-block analogues. There exist the expected manifold of U 6d orbitals of t_{2g} (π^*) and e_g (σ^*) symmetries, and also a 5f orbital manifold at lower energy consisting of a_{2u} (nonbonding), t_{2u} (π), and t_{1u} (σ^* + π^*) symmetric orbitals (Figure 5).

Based on this simple picture, the Cl K-edge XAS of UCl_6^{2-} could exhibit transitions from Cl 1s orbitals into 6d orbitals of t_{2g} and e_g symmetry—as observed for the d-block metals—and additional transitions into empty or partially occupied U 5f orbitals of t_{1u} and t_{2u} symmetry. Hence, the low-energy pre-edge feature in UCl_6^{2-} (2822.41 eV) can be described to a first approximation as involving overlapping transitions into the U 5f orbitals of t_{2u} and t_{1u} symmetry, followed at higher energy by

dx.doi.org/10.1021/ja2105015 | J. Am. Chem. Soc. 2012, 134, 5586−5597

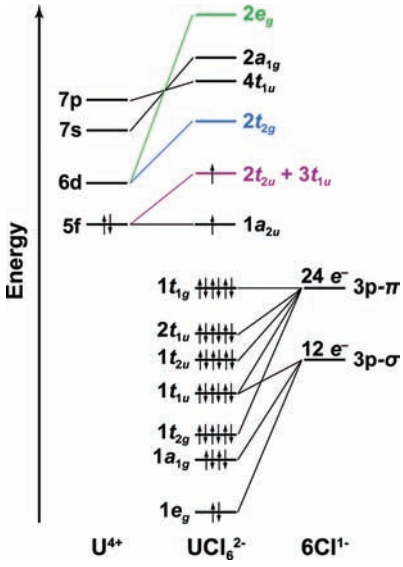

Figure 4. Qualitative molecular orbital diagram for UCl_6^{2-}.

a feature (2823.88 eV) associated with transitions involving the U 6d orbitals of t_{2g} symmetry. From these assignments, the experimental energy separation of the 5f to 6d orbital manifolds (1.47 eV) is found to be in reasonable agreement with the $5f^36d^0 \rightarrow 5f^26d^1$ transition energy observed in optical spectra of U^{3+}-containing systems (ca. 1.8 eV).[67,68] The 6d orbitals of e_g symmetry are calculated at even higher energy, and any associated transitions cannot be resolved from the rising edge, but may be associated with the high-energy shoulder identified in the second-derivative spectrum (see Supporting Information).

It is important to note that the XAS spectral interpretation for UCl_6^{2-} is overly simplistic because it does not take into account effects resulting from spin–orbit coupling and multiple excited-state electron configurations, which are known to be important for accurate description of optical spectra.[42,65,69–71] Spin–orbit coupling ($\zeta \approx 0.2$ eV for U^{4+})[69,71] and multiple excited-state electron configurations will produce a large number of excited states that cannot be experimentally resolved in the Cl K-edge XAS of UCl_6^{2-}. While computational methods that will support a detailed interpretation of these effects are currently in development, the simple electronic structure model presented here supports identification of both 5f and 6d orbital participation in U–Cl bonding for UCl_6^{2-} by Cl K-edge XAS.

The electronic structure of $UOCl_5^-$ was investigated using DFT to provide additional confidence that transitions associated with both the 5f and 6d orbitals could be independently resolved for UCl_6^{2-}. The electronic structure of hexavalent $UOCl_5^-$ (f^0d^0) has been analyzed in detail previously[16,22,72] and is quite different from that of tetravalent UCl_6^{2-} (f^2d^0) given that it has Cl atoms in two unique chemical environments: one *trans* to the oxygen atom with a short U–Cl distance ($U-Cl_{trans}$ = 2.433(2) Å), and four in the equatorial plane with longer U–Cl distances ($U-Cl_{cis}$ = 2.536(1) Å).[73] To facilitate interpretation of the ground-state DFT calculations, it is instructive to trace the origin of the valence molecular orbitals in $UOCl_5^-$ from those in UCl_6. Substitution of one chloride for an oxo ligand reduces the symmetry from O_h to C_{4v}, as depicted in Figure 3, and lifts the degeneracy of the e and t orbitals. This splits the 6d t_{2g} orbitals into $e + b_2$ symmetries and the e_g into $a_1 + b_1$ symmetries (Figure 3). For the U 5f orbitals, the t_{1u} transforms as $e + a_1$, the t_{2u} as $b_1 + e$, and the a_{2u} orbital remains nonbonding with b_2 symmetry. Spin and orbital symmetry allowed transitions can be to either ^1E or $^1A_1$ excited states of $UOCl_5^-$. Remarkably, five features are resolved in the experimental spectrum, which is consistent with the correlation diagram (Figure 3) and calculated orbital energies (Table 2). This analysis suggests that the three low-energy pre-edge features (<2823 eV) in the Cl K-edge XAS of $UOCl_5^-$ are associated with transitions involving 5f orbitals (derived from t_{2u} and t_{1u} in UCl_6) and that the two high-energy features (>2823 eV) are associated with transitions involving low-lying 6d orbitals (derived from t_{2g} in UCl_6). Transitions associated with the remaining U 6d orbitals (derived from e_g in UCl_6) are at high energy and are not experimentally resolvable from the rising edge.

Hybrid TD-DFT Spectral Simulations. The Cl K-edge XAS for the d-block MCl_6^{2-} complexes were calculated using TD-DFT for comparison with the experimental data. This approach has been successfully applied to several transition metal systems to help guide and lend validity to spectral interpretations.[49,53,57,74,75] The simulated spectra for MCl_6^{2-} (Ti, Zr, Hf) are shown in Figure 6. Each simulated spectrum has been shifted by approximately +64 eV to account for omission of atomic and extra-atomic relaxation associated with the core excitation, relativistic stabilization, and errors associated with the functional, as described in the Experimental Section.[76,77] The TD-DFT simulations for the MCl_6^{2-} (Ti, Zr, Hf) complexes show two electronic excitations from Cl 1s orbitals into predominantly metal-based d orbitals of t_{2g} and e_g symmetries, and are in excellent agreement with the experimental spectra (Figure 6). The TD-DFT simulated spectrum of $TiCl_6^{2-}$ also provides confidence that the third high-energy feature (2823.60 eV) is a legitimate component of the experimental spectrum. As previously observed in many transition metal complexes,[54,78–80] the TD-DFT results attribute the origin of this feature to transitions involving orbitals that result from small amounts of mixing between the Cl 3p and higher lying Ti 4d orbitals and do not reflect ground-state bond covalency.

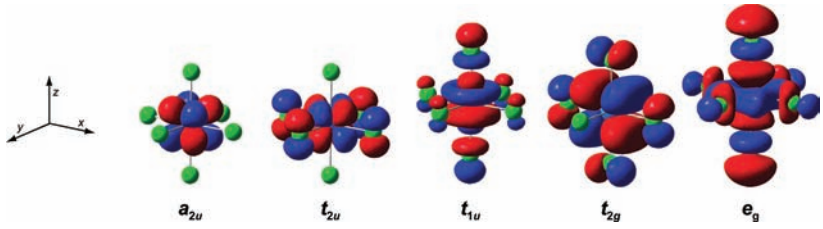

Figure 5. Representative virtual Kohn–Sham orbitals for UCl_6^{2-}. For a complete table of all the virtual Kohn–Sham orbitals for UCl_6, UCl_6^{2-}, and $UOCl_5^-$, refer to the Supporting Information.

dx.doi.org/10.1021/ja2105015 | J. Am. Chem. Soc. 2012, 134, 5586–5597

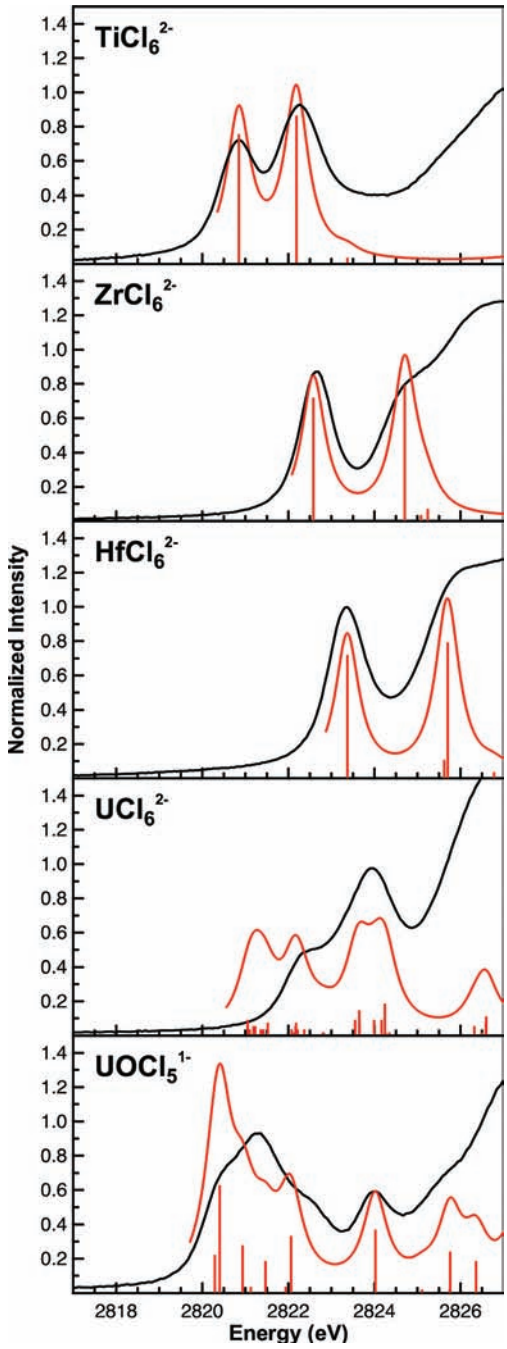

Figure 6. Cl K-edge X-ray absorption spectra for MCl_6^{2-} (M = Ti, Zr, Hf, U; black), the TD-DFT simulated spectra (red), and calculated transitions (red bars). The absolute energy for the TD-DFT calculated transitions and simulated spectra is adjusted based on experimental data, and the height of the calculated transitions gives the relative oscillator strengths (see Experimental Section).

Energies and oscillator strengths for the Cl 1s transitions in the UCl_6^{2-} spectrum were also calculated with TD-DFT. This calculation reproduces the essential pre-edge features in the experimental spectrum, and is consistent with the earlier interpretation (Figure 6). It is important to note that, because the ground state is an open-shell triplet, there are a number of f^3 final states corresponding to different multiplet couplings. In order to span this space completely, determinants are necessary that would not be included in a simple one-electron TD-DFT approach with no spin-flip terms. However, the TD-DFT energies and oscillator strengths correspond to a weighted average over final-state multiplets, and provide a first approximation to the final state spectrum. These neglect higher order excitations and contributions from the α and β spin-orbitals, which can cause the peaks in the TD-DFT simulated spectra to broaden or even split. The TD-DFT simulations show that the lowest-energy experimental feature at 2822.41 eV is attributed to overlapping transitions from Cl 1s orbitals to U 5f orbitals of both t_{2u} and t_{1u} symmetries, and the high-energy pre-edge feature at 2823.88 eV is assigned to a transition from Cl 1s orbitals to the π-antibonding U 6d orbitals of t_{2g} symmetry. Transitions to the σ-antibonding U 6d orbitals of e_g symmetry are calculated to be even higher in energy (2826.56 eV), which is past the onset of the rising edge. A pre-edge feature corresponding to these transitions was not resolved in the experimental Cl K-edge XAS of UCl_6^{2-}, but may be associated with the weak shoulder observed on the post-edge at 2826.25 eV. Overall, the TD-DFT calculations are in agreement with the experimental Cl K-edge XAS for MCl_6^{2-} (Ti, Zr, Hf, U) and aid in the identification of transitions associated with M d orbitals of t_{2g} symmetry as they increase in energy from 3d < 4d < 5d < 6d (Table 2). This assignment is essential, as it identifies the position of the peak associated with the U 6d t_{2g} orbitals in UCl_6^{2-}, and provides further confidence that the lowest-energy transition in the UCl_6^{2-} spectrum is due to Cl 1s transitions into U 5f orbitals of t_{1u} and t_{2u} symmetries.

Peak assignments for UCl_6^{2-} are further validated by comparisons with $UOCl_5^-$. The TD-DFT spectral simulation for $UOCl_5^-$ predicts two high-energy pre-edge features involving U 6d orbitals of b_2 and e symmetries, and three overlapping low-energy features (between ca. 2820 and 2823 eV) that involve the U 5f orbitals of b_1, e, e, and a_1 symmetries (Figure 6). While the TD-DFT calculated energy for the transition associated with the second set of U 5f orbitals of e symmetry (derived from t_{1u} in O_h) subtly differs from the experimental value, the relative peak intensities and peak positions for the other transitions are in good agreement with experiment. In addition, both theory and experiment show that the transition into the orbital of a_1 symmetry will be the highest-energy transition associated with any of the 5f orbitals. Indeed, the Cl 1s $\rightarrow$ a_1 transition appears in the TD-DFT simulated spectrum at 2822.09 eV and is found experimentally at 2822.57 eV (Figure 6 and Table 1).

Evaluation of M−Cl Orbital Mixing. The percentage of Cl 3p character mixed with virtual M orbitals (f or d) for MCl_6^{2-} (M = Ti, Zr, Hf, U) and $UOCl_5^-$ was determined using the well-established D_{2d}-Cs_2CuCl_4 intensity standard developed by Solomon and co-workers.[50] The Cl K-edge XAS of D_{2d}-Cs_2CuCl_4 has a single pre-edge peak with an intensity of 0.53 that corresponds to 7.5% Cl 3p character per Cu−Cl bond. For $TiCl_6^{2-}$, the two pre-edge features associated with the t_{2g} and e_g antibonding orbitals were evaluated with high confidence using the curve-fitting model described above and yield intensities of 0.58(3) and 0.99(5), which correspond to 8.3(4) and 14(1)% Cl 3p character per Ti−Cl bond in the t_{2g} and e_g antibonding orbitals, respectively (Table 2). These experimental values sum to 22(1)% total Cl 3p character per Ti−Cl bond, which is similar to previously reported values for $TiCl_4$ (37%),[49] $(C_5H_5)TiCl_3$ (32%),[49] $(C_5H_5)_2TiCl_2$ (25%),[49,53] and $(C_5Me_5)_2TiCl_2$ (25%).[57] They are also in reasonable agreement with the orbital compositions obtained from the Mulliken population analysis, which have only small amounts of Cl 3p

dx.doi.org/10.1021/ja2105015 | J. Am. Chem. Soc. 2012, 134, 5586−5597

character (12.3 and 11.1% per Ti−Cl bond for t_{2g} and e_g, respectively)

For d orbital mixing, experimental comparisons across the series of MCl_6^{2-} (M = Ti, Zr, Hf, U) are restricted to the orbitals of t_{2g} symmetry, because transitions associated with orbitals of e_g symmetry were not resolved for all four complexes. Here the experimental values show an increase in the Cl 3p and metal d orbital mixing for the π-interaction of t_{2g} symmetry, with the % Cl 3p character increasing from 8.3(4), 10.3(5), 12(1), to 18(1)% as the principal quantum number (n) of the metal d orbitals on Ti, Zr, Hf, and U increases. This increase in orbital mixing is surprising, especially for U, and is discussed in more detail in the Concluding Remarks. In contrast, the ground-state DFT calculations predict that the amount of M−Cl mixing in the orbitals of t_{2g} symmetry should decrease with increasing n (Table 2). While we are not able to compare the total Cl 3p character per M−Cl bond for d orbitals in MCl_6^{2-} experimentally, the calculated amounts are 23.4, 19.8, 18.4, and 12.2% for Ti, Zr, Hf, and U, respectively. For UCl_6^{x-} (x = 0, 2) the calculations also reveal significant changes in the total d orbital mixing as a function of oxidation state, where the total calculated Cl 3p mixing with the U 6d orbitals is 20.5 and 12.2% for UCl_6 and UCl_6^{2-}, respectively. Finally, the experimental data for UCl_6^{2-} reveal that Cl 3p mixing with U 5f orbitals is rather small, with the total for all 5f orbitals being only 5.7(3)% per bond.

The relative roles of the U 5f and 6d orbitals for $UOCl_5^-$ are significantly different from those observed for UCl_6^{2-}. For $UOCl_5^-$ the total amount of Cl 3p character mixed with the six U 5f antibonding orbitals was experimentally determined to be 26(1)% per U−Cl bond. This value is appreciably higher than the 7.3(4) % Cl 3p character experimentally determined for the 6d orbitals of b_2 and e symmetries, which is similar to the calculated value of 7.0%. Not all transitions involving the U 6d orbitals were resolved experimentally, which precludes a comprehensive comparison of experimentally determined 5f and 6d orbital mixing. However, the calculated values can be compared and predict that the total mixing of the Cl 3p orbitals will be 47.3 and 17.2% per Cl bond to the U 5f and 6d orbitals, respectively. This enhancement in Cl 3p mixing with the U 5f orbitals in $UOCl_5^-$ may be related to a more covalent axial U−Cl bond arising from the inverse *trans*-influence of the oxo ligand—a phenomenon which has been detailed in several experimental and theoretical investigations.[16,22,72]

CONCLUDING REMARKS

Understanding the relative roles of the 5f and 6d orbitals in actinide−ligand bonding represents a long-standing experimental and computational challenge. The Cl K-edge XAS results presented here for MCl_6^{2-} (M = Ti, Zr, Hf, U) and $UOCl_5^-$ provide new spectroscopic evidence for the involvement of both 5f and 6d orbitals in actinide-ligand bonding. Pre-edge features in the spectrum of UCl_6^{2-} associated with transitions into the U 6d orbitals of t_{2g} symmetry were identified by comparison with d-block MCl_6^{2-} analogues. A trend of increasing Cl 3p mixing into these metal d orbitals was observed as they became more diffuse with increasing principle quantum number (n): $TiCl_6^{2-}$, 8.3(4)%; $ZrCl_6^{2-}$, 10.3(5)%; $HfCl_6^{2-}$, 12(1)%; UCl_6^{2-}, 18(1)%. This increase in experimental intensity for the open-shell $5f^2$ configuration of UCl_6^{2-} is surprising and may be associated with spin−orbit coupling and multiplet effects that can give rise to additional transitions that are not predicted by hybrid DFT calculations. We note that for $UOCl_5^-$, which has a closed-shell $5f^0$ configuration, no excited-state multiplet effects are possible, and there is excellent correspondence between the calculated and experimentally determined orbital mixing. The origin of this discrepancy is currently being investigated as part of an ongoing study including $ThCl_6^{2-}$ ($5f^0$), UCl_6^{2-} ($5f^2$), $NpCl_6^{2-}$ ($5f^3$), and $PuCl_6^{2-}$ ($5f^4$).

The assignment of low-energy features in the Cl K-edge XAS of O_h-UCl_6^{2-} and C_{4v}-$UOCl_5^-$ to transitions into orbitals of 5f parentage provides unambiguous evidence of U 5f−Cl 3p covalent mixing. These new data add to a growing body of work suggesting that accurate models of electronic structure should account for some covalence in actinide−ligand bonds.[15,36] A simple theoretical framework for understanding these observations begins with an ionic $M^{4+}-Cl^-$ model. In this ionic limit, there is no mixing among the valence orbitals, and no pre-edge features would be observed in the XAS. Deviations from the ionic limit can be addressed with perturbation theory. If the metal orbital is given by ϕ_M, characterized by an orbital energy E_M, and the ligand orbital as $\phi_L(E_L)$, then the mixing between the two can be described by

$$\Psi = \frac{(\phi_M + \lambda\phi_L)}{\sqrt{1 + 2\lambda S_{ML} + \lambda^2}} \quad (1)$$

where S_{ML} is the overlap integral, and the mixing coefficient λ is given to first order by

$$\lambda = \frac{H_{ML}}{E_M^0 - E_L^0} \quad (2)$$

While the off-diagonal matrix element H_{ML} can take various forms depending on the electronic structure model, λ is directly related to S_{ML}. In extended Hückel theory,[81] H_{ML} is proportional to S_{ML} for the two fragment orbitals.

Recall that the intensity of pre-edge transitions in the Cl K-edge XAS is directly related to the orbital mixing coefficient (λ). A nonzero value for λ measures the covalent portion of the bond, in the original sense of Heitler and London.[82] The limit, λ = 1, is characterized by homonuclear diatomics such as H_2 at its equilibrium distance. Note that the wave function for this classic covalently bonded molecule has only 50% covalent character in the Heitler−London sense $H^\bullet-H^\bullet$. The remaining 50% of the molecular orbital corresponds to ionic H^+-H^- and $H^-−H^+$ terms.

For intermediate values of λ there are two important conclusions from eq 2. First, a covalent interaction may be realized in two ways: either by a significant matrix element (H_{ML}) indicative of increased overlap, which can be thought of as overlap driven covalency, or by a vanishing denominator (E_M^0—E_L^0), which is best regarded as near degeneracy driven covalency. The term "covalence" is typically associated with a buildup of charge at the midpoint of the bond due to overlapping orbital densities. It is also possible to induce a covalent interaction by making the denominator in eq 2 small. This would not necessarily be accompanied by a buildup of charge at the midpoint, but would be a covalent interaction, nevertheless.[82]

Second, covalent interactions due to orbital mixing are not always accompanied by a large orbital energy stabilization, or

dx.doi.org/10.1021/ja2105015 | J. Am. Chem. Soc. 2012, 134, 5586−5597

stronger bonds.[17] The energy associated with covalent mixing is given by second-order perturbation theory.

$$\Delta E = \frac{|H_{ML}|^2}{E_M^0 - E_L^0} = \lambda H_{ML} \quad (3)$$

This expression makes clear that two bonds with identical orbital mixing parameters (λ) can have quite different covalent contributions to the bond energies, depending on the magnitude of the Hamiltonian matrix elements (H_{ML}).

Overall, these results show that both 5f and 6d orbitals of U can be involved in U−Cl bonding, and suggest that trends in 5f and 6d orbital mixing are complex and can vary depending on the oxidation state of the metal and the identity of supporting ligands. Future studies to assess the utility of this concept with other MCl_6^{n-} (M = Th, U, Np, Pu) systems are in progress.

EXPERIMENTAL SECTION

General Considerations. MCl_6^{2-} (M = Ti, Zr, Hf, U) and $UOCl_5^-$ were prepared with non-coordinating organic countercations (i.e., Ph_4P^+, Et_4N^+, and Bu_4N^+) in large quantities, isolated as highly pure crystalline solids as previously described, and characterized by single-crystal X-ray diffraction prior to use.[58,83] All sample manipulations were conducted under helium with exclusion of air and water by standard Schlenk, glovebox, and glovebag techniques. Toluene was distilled from sodium and benzophenone and degassed by three freeze−pump−thaw cycles. Polystyrene (PolySciences Inc.) was acquired as 3.0 Micron Dry Form and dried under vacuum (10^{-3} Torr) for 24 h. The polystyrene was verified to contain no chlorine by Cl K-edge XAS. The D_{2d}-Cs_2CuCl_4 intensity and energy calibration standard[46,47,50,59,84,85] was prepared as previously described.[86]

Polystyrene Sample Preparation. *$(Ph_4P)_2TiCl_6$.* Encapsulation in a polystyrene matrix was achieved by a slight modification of the previously described procedure.[53,57] The polystyrene sample was prepared by finely grinding $(Ph_4P)_2TiCl_6$ (6.6 mg) with 3 μm polystyrene beads (120 mg) using a wiggle bug equipped with a polycarbonate ball and container into a mixture which contained 5.5% analyte by weight. An aliquot of this mixture (13 mg) was transferred to a vial that contained additional polystyrene beads (68 mg). This new diluted mixture contained 0.88% analyte by mass, and was ground with a wiggle bug again for 2 min to achieve small and finely divided particles. The entire mixture was transferred to a vial, and toluene (400 μL) was added. The mixture was stirred with a thin glass rod until the solids had dissolved, and the solution was transferred into a 5 × 10 × 4 mm slot that had been bored into an aluminum sample plate, which had been secured to a Teflon block. The toluene was evaporated under the ambient helium atmosphere of the glovebox over 48 h, leaving a robust film fixed in the sample plate window that contained 4.4 μmol of Cl atoms.

$(Ph_4P)_2ZrCl_6$. This sample was prepared in as described for $(Ph_4P)_2TiCl_6$ using, for the first mixture, $(Ph_4P)_2ZrCl_6$ (6.6 mg) and 3 μm polystyrene beads (120 mg). For the second mixture, an aliquot of the first mixture (14 mg) was diluted in additional polystyrene beads (69 mg). The resulting film contained 4.3 μmol of Cl atoms.

$(Ph_4P)_2HfCl_6$. This sample was prepared as described for $(Ph_4P)_2TiCl_6$ using, for the first mixture, $(Ph_4P)_2HfCl_6$ (7.0 mg) and 3 μm polystyrene beads (120 mg). For the second mixture, an aliquot of the first mixture (15 mg) was diluted in additional polystyrene beads (67 mg). The resulting film contained 4.3 μmol of Cl atoms.

$(Ph_4P)_2UCl_6$. This sample was prepared as described for $(Ph_4P)_2TiCl_6$ using, for the first mixture $(Ph_4P)_2UCl_6$ (7.0 mg) and 3 μm polystyrene beads (120 mg). For the second mixture an aliquot of the first mixture (10 mg) was diluted in additional polystyrene beads (70 mg). The resulting film contained 3.5 μmol of Cl atoms.

$(Et_4N)UOCl_5$. This sample was prepared as described for $(Ph_4P)_2UCl_6$ using exactly the same masses of analyte and polystryrene beads. The resulting film contained 3.7 μmol of Cl atoms.

XAS Measurement. All data were measured at the Stanford Synchrotron Radiation Lightsource under ring conditions of 3.0 GeV and 60−100 mA, as described previously.[53,57] Data were measured using the 54-pole wiggler beamline 6.2 in high magnetic field mode of 10 kG with a nickel-coated harmonic rejection mirror detuned by 50% (3150) and a Si(111) double-crystal monochromator. A chamber, similar to that previously described,[50] was used with the exception that the chamber consisted of three compartments which were used for safe containment of the radioactive samples. The sample compartment was separated from the I_0 compartment by a 13.5 μm polypropylene film. The I_0 compartment was isolated from the He-filled compartment with a beryllium window. The sample and I_0 compartments were evacuated and the pressure maintained below 10^{-7} Torr using ion pumps. The sample fluorescence was measured against the incident beam using pairs of International Radiation Detector XUV100 type photodiodes coated with 1000 Å of aluminum. The photodiodes were mounted at normal incidence to the oncoming beam, closely spaced so that the 1−2 mm wide beam passed between them, and fluorescence was collected over a wide solid angle because of its 5−10 mm proximity to the sample. Incident beam intensity was measured using either the scatter off of the polypropylene window with a photodiode pair in the I_0 compartment or using an ion chamber housed in the He-filled compartment. The energy scale was calibrated to 2820.20 eV using the maximum of the first pre-edge feature in the Cl K-edge XAS of the D_{2d}-Cs_2CuCl_4 standard, which was repeatedly analyzed between sample scans.

Data for $(Ph_4P)_2TiCl_6$ and $(Ph_4P)_2HfCl_6$ were collected at room temperature with three different step sizes such that energy steps of 2.00, 0.06, and 3.00 eV were used between 2702.14−2802.14, 2802.14−2852.17, and 2852.17−3140.14 eV, respectively. Data for $(Ph_4P)_2ZrCl_6$ were also collected at room temperature, but with four different step sizes such that energy steps of 4.00 0.07, 0.61, and 3.92 eV were used between 2705.01−2805.01, 2805.01−2835.01, 2835.01−2905.01, and 2905.01−3140.01. Data for $(Ph_4P)_2UCl_6$ and (Et_4N)-$UOCl_5$ were collected with three different step sizes, which were 4.000, 0.072, and 3.899 eV for the pre-edge (2705—2801 eV), edge (2801—2835 eV), and post-edge (2835—3140 eV) regions, respectively. To obtain adequate statistics, 3 or 4 s counting times were employed, and the spectra were collected at least twice. Spectra showed no signs of radiation damage and were reproduced over multiple regions of the sample.

Data Analysis. Data manipulation and analysis was conducted as previously described by Solomon and co-workers.[50] In a typical example, a line was fit to the pre-edge region, 2702.1−2815 eV, and then subtracted from the experimental data to eliminate the background of the spectrum. The data were normalized by fitting a first-order polynomial to the post-edge region of the spectrum, 2836−3030 eV, and setting the edge jump at 2836 eV to an intensity of 1.0. This normalization procedure gives spectra normalized to a single Cl atom or M−Cl bond. Fits to the Cl K-edges were performed using the program IGOR 6.0 and a modified version of EDG_FIT.[87] Second-derivative spectra were used as guides to determine the number and position of peaks. Pre-edge and rising-edge features were modeled by pseudo-Voigt line shapes and a step function. For the pre-edge and white line features, a fixed 1:1 ratio of Lorentzian to Gaussian contributions was used, and for the step function, a 1:1 ratio of arctangent and error function contributions was employed. Fits were performed over several energy ranges. For the spectra of $(Ph_4P)_2MCl_6$ (M = Ti, Zr, Hf), placement of the step function in a variety of positions in the post-edge region had no significant impact on the correlation of the fit to the experiment, or the energy and intensity of the model in the pre-edge region. For consistency, the step position was optimized near that previously observed for $(C_5Me_5)_2MCl_2$ (M = Ti, Zr, Hf).[57] Assignment of merit for the curve fit was given by inspection of the residual intensity, which is obtained by subtracting the fit from the experiment and should resemble a horizontal line at zero (see Supporting Information). The areas under the pre-edge

dx.doi.org/10.1021/ja2105015 | J. Am. Chem. Soc. 2012, 134, 5586−5597

peaks (hereafter defined as the intensity) are equal to the fwhm × PH [where fwhm = full width at half-maximum height (eV); PH = peak height (normalized intensity)] and have error of ±5%, as determined from the standard deviation of the curve fit. Each intensity was compared to that of the well-established Cl K-edge intensity standard D_{2d}-Cs_2CuCl_4. Solomon and co-workers report this feature with a normalized pre-edge intensity of 0.53 corresponding to 7.5% Cl 3p character.[50] Using polystyrene encapsulation methodology, these pre-edge intensities are reproduced routinely between 0.50 and 0.55. Therefore, the amount of Cl 3p character is determined to ±5%.

Electronic Structure Calculations. Ground-state electronic structure calculations were performed on the MCl_6^{2-} (M = Ti, Zr, and Hf) and $UOCl_5^-$ complexes using B3LYP hybrid density functional theory (DFT)[88,89] in the Gaussian 09 code.[90] For the ground-state triplet UCl_6^{2-}, the unrestricted version of the same methods was employed. In an unrestricted calculation the two density matrices can differ because the SCF is carried out separately for the α and β spins, which can result in different molecular orbitals for α and β (referred to as α and β spin-orbitals). The Stuttgart 97 relativistic effective core potential and associated basis sets (without the most diffuse function) were used for U,[12,91,92] while Ti, Zr, and Hf were modeled with the LANL2DZ effective core potential and basis set[93] augmented with the addition of f-polarization functions (exponents =1.506, 0.875, and 0.784).[94] Cl and O were modeled using a Pople style double-ζ 6-31G(d′) basis set with polarization functions optimized for heavy atoms.[95−97] Spin−orbit interactions were not included in the calculations. These functionals and basis sets have been extensively tested for organometallic and inorganic systems and shown to give good agreement with experimental data.[98,99] The populations of the Cl 3p orbitals of each complex were then obtained by Mulliken population analysis of each particular molecular orbital. For comparison with the experiment, calculated values of the percent Cl 3p character in a molecular orbital were normalized to per-bond values by multiplying the total Cl 3p character by the sum of the squares of the normalization constants for the corresponding ligand-orbital wave functions. For example, the 14.4% Cl 3p found in the triply degenerate set of t_{2g} molecular orbitals for UCl_6 was corrected by $(^1/_2)^2 + (^1/_2)^2 + (^1/_2)^2 = {}^3/_4$ in accordance with the equations for the ligand orbitals corresponding to the d_{xy}, d_{xz}, and d_{yz} metal orbitals, which are $^1/_2(x_1 + y_2 + y_3 + x_4)$, $^1/_2(y_1 + x_5 + x_3 + y_6)$, and $^1/_2(x_2 + y_5 + y_4 + x_6)$, respectively.[2,100] Where a given molecular orbital was found to have both σ- and π-bonding character (e.g., the t_{1u} orbitals of 5f parentage), the σ- and π-bonding components were normalized independently first and then summed together to provide the calculated per-bond values in Tables 1 and 2.

Simulated Cl K-edge Spectra. For the MCl_6^{2-} and $UOCl_5^-$ anions, the Cl K-edge XAS was simulated using TD-DFT. These calculations were conducted as previously described.[53,54,57] Specifically, this analysis involves a linear response calculation for extracting the transition amplitudes from the transition densities and dipole moments between the calculated excited states and the ground states. The excitations originating from all of the intermediate states between the Cl 1s and the HOMO were excluded so that only excitations from the core levels to virtual molecular orbitals could be analyzed. This allows the virtual orbitals to relax under the influence of the chlorine core hole, but not the occupied orbitals. Although excluding relaxations in the occupied space results in large errors associated with absolute calculated transition energies, the relative energies address the first-order changes in virtual orbitals accompanying the core hole excitation. As discussed previously,[57] an energy shift must be established to account for the omission of the atomic and extra-atomic relaxation associated with the core excitation, relativistic stabilization, and errors associated with the functional. This was achieved by setting the energy of transitions simulated for the 6d orbitals to be equal to those in the experimental spectra, which resulted in energy shifts of +64.18, +64.63, +64.67, +63.68, and +63.69 eV for $TiCl_6^{2-}$, $ZrCl_6^{2-}$, $HfCl_6^{2-}$, UCl_6^{2-}, and $UOCl_5^-$, respectively.

■ ASSOCIATED CONTENT

Supporting Information

Complete ref 90, additional X-ray absorption spectra and analysis. This material is available free of charge via the Internet at http://pubs.acs.org.

■ AUTHOR INFORMATION

Corresponding Author

stosh@lanl.gov

Notes

The authors declare no competing financial interest.

■ ACKNOWLEDGMENTS

The authors are grateful to N. M. Edelstein, S. DeBeer George, N. Kaltsoyannis, and W. W. Lukens for helpful discussions. This work was supported under the Heavy Element Chemistry Program at LANL by the Division of Chemical Sciences, Geosciences, and Biosciences, Office of Basic Energy Sciences, U.S. Department of Energy. Parts of this work were supported by the Director, Office of Science, Office of Basic Energy Sciences, Division of Chemical Sciences, Geosciences, and Biosciences of the U.S. Department of Energy at Lawrence Berkeley National Laboratory under contract DE-AC02-05CH11231. Parts of this work were also supported at LANL by Glenn T. Seaborg Institute Postdoctoral Fellowships (S.G.M., P.Y.) and Director's Postdoctoral Fellowships (J.M.K.). Portions of this research were carried out at the Stanford Synchrotron Radiation Lightsource, a national user facility operated by Stanford University on behalf of the U.S. Department of Energy, Office of Basic Energy Sciences. Los Alamos National Laboratory is operated by Los Alamos National Security, LLC, for the National Nuclear Security Administration of the U.S. Department of Energy under contract DE-AC52-06NA25396.

■ REFERENCES

(1) Ball, P. *Nature* **2011**, *469*, 26.
(2) Cotton, F. A. *Chemical Applications of Group Theory*, 3rd ed.; John Wiley & Sons: New York, 2004.
(3) DeKock, R. L.; Gray, H. B. *Chemical Structure and Bonding*; University Science Books: Sausalito, CA, 1989.
(4) Figgis, B. N.; Hitchman, M. A. *Ligand Field Theory and Its Applications*; Wiley-VCH: New York, 2000.
(5) Albright, T. A.; Burdett, J. K.; Whangbo, M. *Orbital Interactions in Chemistry*; John Wiley and Sons: New York, 1985.
(6) Raymond, K. N.; Eigenbrot, C. W. *Acc. Chem. Res.* **1980**, *13*, 276.
(7) Krinsky, J. L.; Minasian, S. G.; Arnold, J. *Inorg. Chem.* **2011**, *50*, 345.
(8) Beitz, J. V.; Liu, G. In *The Chemistry of the Actinide and Transactinide Elements*, 3rd ed.; Morss, L., Edelstein, N. M., Fuger, J., Eds.; Springer: Berlin, 2006; Vol. 3, p 2013.
(9) Diamond, R. M.; Street, K.; Seaborg, G. T. *J. Am. Chem. Soc.* **1954**, *76*, 1461.
(10) Tatsumi, K.; Nakamura, A.; Hofmann, P.; Stauffert, P.; Hoffmann, R. *J. Am. Chem. Soc.* **1985**, *107*, 4440.
(11) Pepper, M.; Bursten, B. E. *Chem. Rev.* **1991**, *91*, 719.
(12) Kuchle, W.; Dolg, M.; Stoll, H.; Preuss, H. *J. Chem. Phys.* **1994**, *100*, 7535.
(13) Gagliardi, L.; Willetts, A.; Skylaris, C. K.; Handy, N. C.; Spencer, S.; Ioannou, A. G.; Simper, A. M. *J. Am. Chem. Soc.* **1998**, *120*, 11727.
(14) Schreckenbach, G.; Hay, P. J.; Martin, R. L. *J. Comput. Chem.* **1999**, *20*, 70.
(15) Choppin, G. R. *J. Alloys Compd.* **2002**, *344*, 55.
(16) Straka, M.; Patzschke, M.; Pyykko, P. *Theor. Chem. Acc.* **2003**, *109*, 332.

(17) Barros, N.; Maynau, D.; Maron, L.; Eisenstein, O.; Zi, G.; Andersen, R. A. *Organometallics* **2007**, *26*, 5059.
(18) Prodan, I. D.; Scuseria, G. E.; Martin, R. L. *Phys. Rev. B.* **2007**, 76.
(19) Tassell, M. J.; Kaltsoyannis, N. *Dalton Trans.* **2010**, *39*, 6719.
(20) Kirker, I.; Kaltsoyannis, N. *Dalton Trans.* **2011**, *40*, 124.
(21) Tatsumi, K.; Hoffmann, R. *Inorg. Chem.* **1980**, *19*, 2656.
(22) Denning, R. G. *Struct. Bonding (Berlin)* **1992**, *79*, 215.
(23) Denning, R. G.; Green, J. C.; Hutchings, T. E.; Dallera, C.; Tagliaferri, A.; Giarda, K.; Brookes, N. B.; Braicovich, L. *J. Chem. Phys.* **2002**, *117*, 8008.
(24) Denning, R. G. *J. Phys. Chem. A* **2007**, *111*, 4125.
(25) Zalkin, A.; Raymond, K. N. *J. Am. Chem. Soc.* **1969**, *91*, 5667.
(26) Avdeef, A.; Zalkin, A.; Raymond, K. N.; Hodgson, K. O. *Inorg. Chem.* **1972**, *11*, 1083.
(27) Liu, W. J.; Dolg, M.; Fulde, P. *J. Chem. Phys.* **1997**, *107*, 3584.
(28) Seyferth, D. *Organometallics* **2004**, *23*, 3562.
(29) Kerridge, A.; Kaltsoyannis, N. *J. Phys. Chem. A* **2009**, *113*, 8737.
(30) Clark, J. P.; Green, J. C. *J. Organomet. Chem.* **1976**, *112*, C14.
(31) Green, J. C. *Struct. Bonding (Berlin)* **1981**, *43*, 37.
(32) Brennan, J. G.; Green, J. C.; Redfern, C. M. *J. Am. Chem. Soc.* **1989**, *111*, 2373.
(33) Mazzanti, M.; Wietzke, R. L.; Pecaut, J.; Latour, J. M.; Maldivi, P.; Remy, M. *Inorg. Chem.* **2002**, *41*, 2389.
(34) Mehdoui, T.; Berthet, J. C.; Thuery, P.; Ephritikhine, M. *Dalton Trans.* **2004**, 579.
(35) Gaunt, A. J.; Scott, B. L.; Neu, M. P. *Chem. Commun.* **2005**, 3215.
(36) Choppin, G. R.; Jensen, M. P. In *The Chemistry of the Actinide and Transactinide Elements*; Morss, L., Edelstein, N. M., Fuger, J., Eds.; Springer: Berlin, 2006; Vol. 3, p 2562.
(37) Gaunt, A. J.; Scott, B. L.; Neu, M. P. *Angew. Chem., Int. Ed.* **2006**, *45*, 1638.
(38) Gaunt, A. J.; Scott, B. L.; Neu, M. P. *Inorg. Chem.* **2006**, *45*, 7401.
(39) Gaunt, A. J.; Reilly, S. D.; Enriquez, A. E.; Scott, B. L.; Ibers, J. A.; Sekar, P.; Ingram, K. I. M.; Kaltsoyannis, N.; Neu, M. P. *Inorg. Chem.* **2008**, *47*, 29.
(40) Ingram, K. I. M.; Tassell, M. J.; Gaunt, A. J.; Kaltsoyannis, N. *Inorg. Chem.* **2008**, *47*, 7824.
(41) Daly, S. R.; Klaehn, J. R.; Boland, K. S.; Kozimor, S. A.; MacInnes, M. M.; Peterman, D. R.; Scott, B. L. *Dalton Trans.* **2012**, *41*, 2163.
(42) Kaltsoyannis, N.; Hay, P. J.; Li, J.; Blaudeau, J.-P.; Bursten, B. E. In *The Chemistry of the Actinide and Transactinide Elements*, 3rd ed.; Morss, L., Edelstein, N. M., Fuger, J., Eds.; Springer: Berlin, 2006; Vol. 3, p 1893.
(43) Minasian, S. G.; Krinsky, J. L.; Rinehart, J. D.; Copping, R.; Tyliszczak, T.; Janousch, M.; Shuh, D. K.; Arnold, J. *J. Am. Chem. Soc.* **2009**, *131*, 13767.
(44) Hedman, B.; Hodgson, K. O.; Solomon, E. I. *J. Am. Chem. Soc.* **1990**, *112*, 1643.
(45) Shadle, S. E.; Hedman, B.; Hodgson, K. O.; Solomon, E. I. *Inorg. Chem.* **1994**, *33*, 4235.
(46) Shadle, S. E.; Hedman, B.; Hodgson, K. O.; Solomon, E. I. *J. Am. Chem. Soc.* **1995**, *117*, 2259.
(47) Neese, F.; Hedman, B.; Hodgson, K. O.; Solomon, E. I. *Inorg. Chem.* **1999**, *38*, 4854.
(48) Glaser, T.; Hedman, B.; Hodgson, K. O.; Solomon, E. I. *Acc. Chem. Res.* **2000**, *33*, 859.
(49) George, S. D.; Brant, P.; Solomon, E. I. *J. Am. Chem. Soc.* **2005**, *127*, 667.
(50) Solomon, E. I.; Hedman, B.; Hodgson, K. O.; Dey, A.; Szilagyi, R. K. *Coord. Chem. Rev.* **2005**, *249*, 97.
(51) Hedman, B.; Frank, P.; Gheller, S. F.; Roe, A. L.; Newton, W. E.; Hodgson, K. O. *J. Am. Chem. Soc.* **1988**, *110*, 3798.
(52) Shadle, S. E.; Pennerhahn, J. E.; Schugar, H. J.; Hedman, B.; Hodgson, K. O.; Solomon, E. I. *J. Am. Chem. Soc.* **1993**, *115*, 767.
(53) Kozimor, S. A.; Yang, P.; Batista, E. R.; Boland, K. S.; Burns, C. J.; Christensen, C. N.; Clark, D. L.; Conradson, S. D.; Hay, P. J.; Lezama, J. S.; Martin, R. L.; Schwarz, D. E.; Wilkerson, M. P.; Wolfsberg, L. E. *Inorg. Chem.* **2008**, *47*, 5365.
(54) Bradley, J. A.; Yang, P.; Batista, E. R.; Boland, K. S.; Burns, C. J.; Clark, D. L.; Conradson, S. D.; Kozimor, S. A.; Martin, R. L.; Seidler, G. T.; Scott, B. L.; Shuh, D. K.; Tyliszczak, T.; Wilkerson, M. P.; Wolfsberg, L. E. *J. Am. Chem. Soc.* **2010**, *132*, 13914.
(55) George, S. D.; Huang, K. W.; Waymouth, R. M.; Solomon, E. I. *Inorg. Chem.* **2006**, *45*, 4468.
(56) Ray, K.; George, S. D.; Solomon, E. I.; Wieghardt, K.; Neese, F. *Chem.—Eur. J.* **2007**, *13*, 2783.
(57) Kozimor, S. A.; Yang, P.; Batista, E. R.; Boland, K. S.; Burns, C. J.; Clark, D. L.; Conradson, S. D.; Martin, R. L.; Wilkerson, M. P.; Wolfsberg, L. E. *J. Am. Chem. Soc.* **2009**, *131*, 12125.
(58) Minasian, S. G.; Boland, K. S.; Feller, R. K.; Gaunt, A. J.; Kozimor, S. A.; May, I.; Reilly, S. D.; Scott, B. L.; Shuh, D. K. *Inorg. Chem.* **2012**, in press.
(59) Didziulis, S. V.; Cohen, S. L.; Gewirth, A. A.; Solomon, E. I. *J. Am. Chem. Soc.* **1988**, *110*, 250.
(60) Lever, A. B. P. *Inorganic Electronic Spectroscopy*, 2nd ed.; Elsevier Science: Oxford, 1985.
(61) Brisdon, B. J.; Fowles, G. W. A.; Tidmarsh, D. J.; Walton, R. A. *Spectrochim. Acta A* **1969**, *A 25*, 999.
(62) Brisdon, B. J.; Lester, T. E.; Walton, R. A. *Spectrochim. Acta A* **1967**, *A 23*, 1969.
(63) Fowles, G. W. A.; Russ, B. J. *J. Chem. Soc. a-Inorg. Phys. Theor.* **1967**, 517.
(64) Crouch, P. C.; Fowles, G. W. A.; Walton, R. A. *J. Chem. Soc. a -Inorg. Phys. Theor.* **1969**, 972.
(65) Kaltsoyannis, N.; Bursten, B. E. *Inorg. Chem.* **1995**, *34*, 2735.
(66) The unrestricted Kohn−Sham $5f^2$ ground state breaks symmetry and causes a loss of degeneracy in the t_{2u} and t_{1u} sets, which results in a large energy separation for the a_{2u} orbital and one of the t_{2u} orbitals.
(67) Karbowiak, M.; Drozdzynski, J.; Hubert, S.; Simoni, E.; Strek, W. *J. Chem. Phys.* **1998**, *108*, 10181.
(68) Seijo, L.; Barandiáran, Z. *J. Chem. Phys.* **2003**, *118*, 5335.
(69) Satten, R. A.; Schreibe, Cl; Wong, E. Y. *J. Chem. Phys.* **1965**, *42*, 162.
(70) Edelstein, N. M.; Brown, D.; Whittaker, B. *Inorg. Chem.* **1974**, *13*, 563.
(71) Wagner, W.; Edelstein, N.; Whittaker, B.; Brown, D. *Inorg. Chem.* **1977**, *16*, 1021.
(72) O'Grady, E.; Kaltsoyannis, N. *Dalton Trans.* **2002**, 1233.
(73) Dewet, J. F.; Dupreez, J. G. H. *Dalton Trans.* **1978**, 592.
(74) Casarin, M.; Finetti, P.; Vittadini, A.; Wang, F.; Ziegler, T. *J. Phys. Chem. A* **2007**, *111*, 5270.
(75) George, S. D.; Petrenko, T.; Neese, F. *Inorg. Chim. Acta* **2008**, *361*, 965.
(76) Segala, M.; Chong, D. P. *J. Electron Spectrosc. Relat. Phenom.* **2010**, *182*, 141.
(77) Martin, R. L.; Shirley, D. A. In *Electron Spectroscopy, Theory, Techniques and Applications*; Academic Press: New York, 1977; Vol. *1*, p 75.
(78) Ruhl, E.; Hitchcock, A. P. *J. Am. Chem. Soc.* **1989**, *111*, 5069.
(79) Wen, A. T.; Ruhl, E.; Hitchcock, A. P. *Organometallics* **1992**, *11*, 2559.
(80) Ruhl, E.; Heinzel, C.; Baumgartel, H.; Hitchcock, A. P. *Chem. Phys.* **1993**, *169*, 243.
(81) Hoffmann, R. *J. Chem. Phys.* **1963**, *39*, 1397.
(82) Heitler, W.; London, F. *Z. Phys.* **1927**, *44*, 455.
(83) Bagnall, K. W.; Preez, J.; Gellatly, B. J.; Holloway, J. H. *Dalton Trans.* **1975**, 1963.
(84) Gewirth, A. A.; Cohen, S. L.; Schugar, H. J.; Solomon, E. I. *Inorg. Chem.* **1987**, *26*, 1133.
(85) Shadle, S. E. Ph.D. Thesis, Stanford University, 1994.
(86) Helmholz, L.; Kruh, R. F. *J. Am. Chem. Soc.* **1952**, *74*, 1176.
(87) George, G. N. *EDG_FIT*; Stanford Synchrotron Radiation Laboratory, Stanford Linear Accelerator Center: Stanford, CA.

(88) Becke, A. D. *J. Chem. Phys.* **1993**, *98*, 5648.
(89) Lee, C. T.; Yang, W. T.; Parr, R. G. *Phys. Rev. B* **1988**, *37*, 785.
(90) Frisch, M. J. et al. *Gaussian 09*, Revision B.01; Gaussian Inc.: Wallingford, CT.
(91) Fuentealba, P.; Preuss, H.; Stoll, H.; Vonszentpaly, L. *Chem. Phys. Lett.* **1982**, *89*, 418.
(92) Kuchle, W.; Dolg, M.; Stoll, H.; Preuss, H. *Mol. Phys.* **1991**, *74*, 1245.
(93) Hay, P. J.; Wadt, W. R. *J. Chem. Phys.* **1985**, *82*, 299.
(94) Ehlers, A. W.; Bohme, M.; Dapprich, S.; Gobbi, A.; Hollwarth, A.; Jonas, V.; Kohler, K. F.; Stegmann, R.; Veldkamp, A.; Frenking, G. *Chem. Phys. Lett.* **1993**, *208*, 111.
(95) Francl, M. M.; Pietro, W. J.; Hehre, W. J.; Binkley, J. S.; Gordon, M. S.; Defrees, D. J.; Pople, J. A. *J. Chem. Phys.* **1982**, *77*, 3654.
(96) Harihara, P. C.; Pople, J. A. *Chem. Phys. Lett.* **1972**, *16*, 217.
(97) Krishnan, R.; Binkley, J. S.; Seeger, R.; Pople, J. A. *J. Chem. Phys.* **1980**, *72*, 650.
(98) Niu, S. Q.; Hall, M. B. *Chem. Rev.* **2000**, *100*, 353.
(99) Baker, J.; Muir, M.; Andzelm, J.; Scheiner, A. In *ACS Symposium Series 629*; Laird, B. B., Ross, R. B., Ziefler, T., Eds.; American Chemical Society: Washington, DC, 1996.
(100) Ballhausen, C. J.; Gray, H. B. *Molecular Orbital Theory*; W. A. Benjamin, Inc.: New York, 1965.
(101) Cramer, C. J. *Essentials of Computational Chemistry*, 2nd ed.; Wiley: Chichester, UK, 2004.